HHS Public Access

Author manuscript

Nat Neurosci. Author manuscript; available in PMC 2014 May 01.

Published in final edited form as:

Nat Neurosci. 2013 November ; 16(11): 1701–1708. doi:10.1038/nn.3530.

Computation of linear acceleration through an internal model in the macaque cerebellum

Jean Laurens[1], **Hui Meng**[2], and **Dora E. Angelaki**[2]

[1]Department of Otolaryngology, Washington University School of Medicine, St. Louis, MO

[2]Dept of Neuroscience, Baylor College of Medicine, Houston, TX

Abstract

A combination of theory and behavioral findings has supported a role for internal models in the resolution of sensory ambiguities and sensorimotor processing. Although the cerebellum has been proposed as a candidate for implementation of internal models, concrete evidence from neural responses is lacking. Here we exploit un-natural motion stimuli, which induce incorrect self-motion perception and eye movements, to explore the neural correlates of an internal model proposed to compensate for Einstein's equivalence principle and generate neural estimates of linear acceleration and gravity. We show that caudal cerebellar vermis Purkinje cells and cerebellar nuclei neurons selective for actual linear acceleration also encode erroneous linear acceleration, as expected from the internal model hypothesis, even when no actual linear acceleration occurs. These findings provide strong evidence that the cerebellum might be involved in the implementation of internal models that mimic physical principles to interpret sensory signals, as previously hypothesized by theorists.

Introduction

The brain maintains 'internal models' of the environment to interpret sensory inputs and prepare actions[1–7]. One function of internal models is to resolve sensory ambiguities[5]. In the vestibular system, sensing one's movement during passive motion is complicated by an ambiguity related to Einstein's equivalence principle[8]: linear (inertial) accelerations experienced as one translates in the world are physically equivalent to the gravitational acceleration present whenever one changes orientation (i.e., tilts) relative to earth-vertical. Consequently, otolith afferents in the inner ear encode the net gravito-inertial acceleration (GIA)[9,10]. Theoretical[11–19] and behavioral[5,20] studies have suggested that the brain resolves this ambiguity by using physical principles to implement an internal model of gravity. This model integrates rotation signals from the semicircular canals or vision to track an internal estimate of head orientation relative to gravity. This estimate is then used to extract linear

Address for correspondence: Dr. Dora E. Angelaki, angelaki@bcm.edu, Dept of Neuroscience, Room T504C, MS: BCM295, Baylor College of Medicine, One Baylor Plaza, Houston TX 77030, Phone: 713–798–1468, Fax: 713–798–6228.

Authors contributions: Jean Laurens designed and performed the experiments, analyzed the data and prepared the manuscript. Hui Meng performed experiments. Dora Angelaki designed the experiments and prepared the manuscript.

acceleration through subtraction from the otolith-driven GIA signal, thereby resolving the gravito-inertial ambiguity.

The fact that the brain indeed uses canal-driven signals to compute linear acceleration has been verified through lesion studies[20–22]. Translation-selective neurons have been found in the vestibular and cerebellar nuclei[9], cerebral cortex[23,24] and thalamus[25,26], as well as Purkinje cells in the nodulus/uvula of the caudal cerebellar vermis (lobules X/IX)[22,27]. The cerebellum is often conceptually associated with the implementation of internal models[2,28–31], suggesting that the translation-selective Purkinje cells previously identified[9,22,27] represent the output of the internal model postulated to resolve the gravito-inertial ambiguity[11–19]. But because previous studies used stimuli that consisted of actual tilt and translation movements, this hypothesis could not be tested. Thus, it is presently unknown whether cerebellar responses reflect computations through an internal model, or simpler but computationally inappropriate filtering (Raphan paper). Here we address this question using an experimental protocol that induces an erroneous linear acceleration signal.

Tilt while rotating (TWR, also known as ‘vestibular cross-coupling’ or ‘vestibular Coriolis effect’) is a disorienting and nauseating stimulus in humans commonly used in motion sickness training[32–36]. It consists of tilting the head while rotating continuously around an earth-vertical axis (Fig. 1a; Supplementary Movies 1a and 2a), similar as tilting the head while riding a merry-go-round. Why this stimulus causes dizziness and disorientation is outlined in Fig. 1 (see also Fig. 2 and Modeling section in Supplementary Materials). During continuous rotation, the output of the semicircular canals is attenuated over time. As a result, when the head tilts in pitch during steady-state, an erroneous roll rotation signal is generated in the canals (Fig. 1b and Supplementary Movie 1b,c). According to theory, this roll canal signal is integrated by the internal model to create an ‘erroneous’ roll tilt estimate (as if the head is tilted ear-down; Fig. 1c). Since the head is in fact upright, the output of the internal model of gravity is in conflict with the otolith cues, which signal that GIA is aligned with the head-vertical axis (Fig. 1b–d). The only inference consistent with these signals is that the head is simultaneously translating (Fig. 1d and Supplementary Movie 2b).

Thus, the internal model hypothesis predicts that TWR should induce an erroneous translation signal. Indeed, such induced roll tilt and erroneous translation have both been observed in reflexive eye movements[5,37]. We have reasoned that, if cell responses in the macaque cerebellum reflect these internal model computations, translation-selective neuron activity should also correlate with this erroneous translation signal. Here we test this hypothesis by recording from nodulus/uvula Purkinje cells and deep cerebellar nuclei neurons during TWR.

Theory and Simulations

The disorienting effects of TWR are the consequence of two phenomena: (i) Due to their physical properties, the semicircular canals emit incorrect rotation signals during steady-state (Supplementary Movie 1) and (ii) Because of these erroneous canal signals, the hypothesized internal model generates an erroneous estimate of orientation relative to gravity and, thus, causes an illusory translation (Supplementary Movie 2).

During TWR, the subject tilts back and forth ("pitch" tilt; Fig. 2a–c and Supplementary Movie 1a) relative to a fixed, earth-vertical axis of rotation (EVAR; Fig. 2a and Supplementary Movie 1b). In an egocentric frame of reference, the projection of the EVAR velocity vector (Fig. 2a) on the head's "yaw" (head-vertical) axis (Fig. 2a) is approximately constant (Fig. 2d). In contrast, the projection of the EVAR vector on the head's "roll" (forward-pointing) axis (Fig. 2a) is negative when the head tilts forward and positive when the head tilts backward (Supplementary Movie 1b). As a consequence, the roll component of head velocity reverses (±7.8°/s) with each tilt movement (Fig. 2e). The brain continuously reconstructs the net rotation of the head by summing the yaw and roll velocity signals (Supplementary Movie 1c).

The semicircular canals, however, emit incorrect rotation signals during steady-state because they are sensitive to angular acceleration (i.e. changes in head velocity). During rotation at constant velocity (Fig. 2d), canal responses fade away with a time constant of ~4 s[38] (Fig. 2d,e and Supplementary Movie 1c). The brain has the ability to increase the duration of the rotation signal somewhat (Fig. 2d,e), via a process known as "velocity storage"[17,39]. Nevertheless, after central rotation signals decrease to zero, the resultant rotation signal following each tilt movement is erroneously aligned with the roll axis, i.e. it erroneously indicates a sideward rotation.

The key assumption of the internal model hypothesis (Fig. 3a; see also Supplementary Modeling and Supplementary Fig. 1) is that the brain tracks an *internal model of gravity* through the integration of central rotation signals[11,13,16–19]. A general formula for tracking the gravity vector, G(t), by integrating rotational velocity, Ω(t), in three dimensions is:

$$G(t)=\int G(t)x\Omega(t)\,dt \quad (1)$$

where 'x' denotes the vector cross-product. Translational acceleration can then be extracted as the difference between this gravity estimate and GIA, the signal carried by primary otolith afferents, i.e.,

$$A(t)=G(t)-GIA(t) \quad (2)$$

Ideally, equation (1) would provide an exact estimate of gravity. However, in practice, limitations exist because the semicircular canals do not always provide a reliable rotation signal, as illustrated already in Fig. 2d,e. Any error in the rotation velocity, Ω, would cause an error in the tilt estimate (which is exactly what happens during steady-state TWR). In the absence of a correction system, errors would remain indefinitely and accumulate over time[17]. To avoid severe disorientation, the brain corrects such errors by a feedback loop ("somatogravic feedback"), which slowly but continuously aligns the internal model output with the GIA[16,17]. Incorporating this loop into the model results in equation (1) being replaced by:

$$G(t)=\int G(t)x\Omega(t)\,dt-1/\tau_s\,(G(t)-GIA(t)) \quad (3)$$

where τ_s is the time constant (one of 5 model parameters; see Supplementary Modeling). The rationale behind this process is as follows: in general, the GIA (otolith response) may differ from the output of the gravity estimator (G) because of linear accelerations. However, long duration accelerations are infrequent in everyday life. Hence, long duration mismatch between G and GIA should be corrected by aligning G towards the GIA. The somatogravic feedback reflects the expectation that it is more likely that we are stationary (but tilted) than accelerating in the world. Accordingly, it has also been modeled as a Bayesian prior centered on zero linear acceleration[16,17].

Based on the model of Fig. 3a, the induced roll signal is integrated by the gravity estimator (equation 3) to generate an erroneous roll tilt and, given equation (2), an erroneous translation signal. Without somatogravic feedback, the induced roll velocity signal (see simulation in Fig. 3b) would result in a large erroneous roll tilt (~50°; Fig. 3b, top), thus creating a huge translation estimate (>7.5 m/s^2; Fig. 3b, top), both of which would remain indefinitely. The somatogravic feedback substantially reduces both the magnitude and duration of the induced tilt and erroneous linear acceleration (Fig. 3b, bottom traces).

The simulations shown in Fig. 2f are based on the model of Fig. 3 (see Supplementary Modeling for model parameters). Note that tilt movements delivered at the onset of EVAR (*"initial TWR"*) should not create an erroneous translation (Fig. 2f) because the yaw and roll canal-driven signals decay together, thus indicating a veridical rotation direction (Supplementary Movie 1c). Therefore, by examining differences in the magnitude of responses to initial versus steady-state TWR we can test the hypothesis that the postulated internal model of Fig. 3a uses three-dimensional rotation information, as predicted by the implementation of the vector differential equation (3).

With these predictions in hand, we next examine how translation-selective cells in the nodulus/uvula and cerebellar nuclei respond during TWR. For simplicity, we will refer to each of the components of Fig. 2 as *'actual tilt'* (green), *'induced tilt'* (cyan) and *'induced linear acceleration'* (red). If indeed the cerebellum reflects the output of the postulated internal model to disambiguate gravitoinertial acceleration, we expect translation-selective Purkinje cells to respond during steady-state TWR in line with the simulations of Fig. 2f and 3b (hypothesis #1). Alternatively, if no internal model is used or if cerebellar neuron activity does not reflect these internal model computations, translation-selective cells should not modulate during TWR because there is no actual linear acceleration stimulus. In addition, responses to initial TWR would reveal whether the internal model indeed uses three-dimensional canal signals to compute a veridical estimate of angular velocity (hypothesis #2). If so, these erroneous translation responses should build up gradually as EVAR velocity decays after the initial TWR response. These two hypotheses are quantitatively tested next.

Results

We recorded simple spike activity from nodulus/uvula Purkinje cells[22,27] and from cerebellar nuclei neurons[21] (located mostly in the rostral fastigial nucleus[40,41]) that responded selectively to translation, rather than GIA (recording maps are shown in Supplementary Fig. 2). We recorded from 'Vestibular-only' cells that don't respond to eye

movements. TWR responses from a representative translation-selective nodulus/uvula Purkinje cell[22], which responded vigorously during sinusoidal translation (Fig. 4a) but only weakly during an equivalent roll tilt stimulus (Fig. 4b), are illustrated in Fig. 4c,d. The cell also responded vigorously during TWR, with large increases and decreases in firing rate following every tilt movement (Fig. 4c, d).

Whether firing rate increases or decreases depends on both the direction of tilt (nose-down vs. nose-up; Fig. 4f) and the direction of EVAR (Fig. 4c,d, EVAR traces). During leftward rotation (Fig. 4c), this particular example cell is activated in response to forward (negative) tilt and inhibited in response to backward (positive) tilt. This pattern is reversed during rightward rotation (Fig. 4d). Dependence on the direction of EVAR demonstrates that these responses do not merely represent the tilt movement itself. Accordingly, the cell does not respond to an identical sequence of tilts performed in the absence of EVAR (Fig. 4e). In the following, we will show that this modulation reflects the cell's response to the erroneous translation signal generated during TWR.

Relevant to this analysis are also the characteristic reflexive horizontal eye movements (vestibulo-ocular reflex, VOR) generated during TWR (see also Supplementary Fig. 3). At the onset of constant velocity, a horizontal VOR is elicited that slowly decays to zero (Fig. 4c,d). The direction of this eye velocity response is rightward (negative, Fig. 4c) during leftward EVAR and leftward (positive, Fig. 4d) during rightward EVAR and it does not depend on pitch tilt direction (Supplementary Fig. 3). Thus, the initial horizontal eye velocity is an angular VOR (aVOR) in response to the EVAR. Each subsequent pitch movement generates a vertical aVOR (Fig. 4c–e) and also results in a short-lasting horizontal eye velocity, whose direction depends on both the direction of tilt and the direction of EVAR. In contrast, no horizontal eye velocity is generated without EVAR (Fig. 4e). Indeed, as shown previously[5], these horizontal eye movements reflect a translational VOR (tVOR) in response to the induced translation signal generated according to the internal model schematized in Fig. 3a. Importantly, neither these horizontal eye movements nor the cell's responses (next section) are due to a yaw aVOR signal because (1) the horizontal canals are minimally activated during these tilts (Supplementary Movie 1c and Supplementary Fig. 4) and (2) responses depend on both the direction of tilt and direction of rotation, whereas the yaw aVOR only depends on the latter (see Supplementary Fig. 4).

Our goal is to test whether the cells' responses correlate qualitatively and quantitatively with this erroneous translation signal. We first analyze steady-state responses (more than 30 s after the onset of TWR).

Steady-state responses during TWR

If indeed cell modulation during TWR reflects responses to the erroneous translation signal, we should expect a correlation between the magnitude of the TWR response (Fig. 5a) and the cell's gain during actual translation. Indeed, there was a significant correlation for both TWR in preferred direction (PD) (Fig. 5b; R^2=0.59, F test: $p<10^{-4}$) and anti-PD (Fig. 5c; R^2=0.35, F test: $p<10^{-5}$) responses. Here, 'preferred' direction, PD, is defined as the tilt/EVAR combinations that would theoretically elicit an erroneous translation in the preferred direction of the cell (expected to increase firing rate). Similarly, tilts in anti-PD refer to

movements which elicit an erroneous translation in the opposite direction (expected to decrease firing rate). In contrast, there was no significant response and no correlation during tilts without EVAR (Fig. 5d; R^2=0.003, F test: p=0.7). Nodulus/uvula Purkinje cells and cerebellar nuclei neurons responded similarly (similar regression slopes, see legend and Supplementary Fig. 5). Thus, nodulus/uvula and cerebellar nuclei cell responses are considered together hereafter.

These results suggest that (1) increases and decreases in firing rate time-locked to each tilt movement during steady-state TWR follow qualitatively the sign predicted for the induced translation signal and (2) the response magnitude correlates with the respective translation gain of each cell. Both of these findings are consistent with the hypothesis that translation-selective cerebellar cells carry a signal proportional to the erroneous translation during TWR. The slope of the PD responses was 1.4 [1.1,1.7, 95% CI] m.s^{-2}. For TWR responses in anti-PD, the slope was −0.8 [−1.1, −0.5] m.s^{-2}. These population response slopes can be interpreted as a way to decode the magnitude of the induced translation during steady-state TWR. The decoded value is close to that predicted by the model in Fig. 3a (~1 m.s^{-2}; Fig. 3b).

We also analyzed the time course of the population response to steady-state TWR (Fig. 6a). The population activity decayed with a time constant of 4 s (animal V), 2.2 s (animal T) and 1.3 s (animal K). The anti-PD population responses were weaker, as is often the case for cerebellar neurons[42], and not significant in animals T and K.

The tVOR responses lasted about 20s (Fig. 6b), in close agreement with previous measurements (see Fig. 3e-h in[5]). The dynamics of tVOR responses involve additional temporal filtering that is not included in the simplified model of Fig. 3a4[43,44] (but see Supplementary Fig. 6). The vertical aVOR that compensates for the actual tilt movement, matches the imposed tilt velocity in both magnitude (mean: 18±0.1°/s, SE; i.e., gain of 0.87) and duration (1.4 s). The induced aVOR, which is a direct measure of the induced activation of the canals, reached a similar peak velocity (12±1.3°/s, 11±0.7°/s and 10±0.5°/s in animals V, T and K, respectively; see Supplementary Table 1 and Fig. 6c), corresponding to a gain of ~0.8 relative to the simulated induced signal. However, its time constant varied across animals: 8.3 s (animal V), 3.5 (animal T) and 1.8 s (animal K). Model simulations followed the basic characteristics of both neural responses and induced aVOR (Fig. 6a,c). Finally, note that both the neuronal response and the behavioral output (tVOR) show a sluggish rise because the ‘stimulus’ (i.e., the induced tilt/translation signal) rises slowly over a period of 1.4s (duration of pitch tilt). This slow build-up predicted by the differential filtering of each variable in the model of Fig. 3 is remarkably in line with experimental observations (Supplementary Fig. 6).

Note that the model in Fig. 3a is based on physical and geometrical rules and has only 5 parameters (see Supplementary Modeling). Four parameters are used to describe the canals and the central processing of rotation information[17]. Importantly, these parameters are only used to compute the central rotation signal, Ω(t) which can be observed in the aVOR of each animal. Thus, these 4 model parameters were chosen such that they simulate the evoked eye movement. In the steady-state, Ω(t) is identical to the induced signal, which was reproduced

accurately in all animals (Fig. 6c). Given Ω(t) and the otolith-driven GIA(t), the model computes the acceleration signal, A(t), using equations (3) and (2), with only a single additional free parameter, τ_s, which was set to τ_s = 0.5 s. Remarkably, the simulated acceleration signal closely matched the neuronal population response in all animals (Fig. 6a). This demonstrates that variations in the duration of Ω(t) were sufficient to explain quantitative differences in neural responses across animals. Model simulations also predicted larger induced linear acceleration for 120°/s vs. 45°/s rotations (2.1 vs. 0.9 $m.s^{-2}$, respectively), although increases in neural activity were smaller (1.8±0.7 vs. 1.2±0.6 $m.s^{-2}$; Fig. 6a, rightmost column), possibly suggesting some saturation effect.

Time course of induced linear acceleration: Influence of yaw rotation signals

In the previous section, quantification of the responses obtained during steady-state TWR provides support for hypothesis #1. It is known, however, that TWR does not have any disorienting effect if the tilt movement is performed shortly after the beginning of EVAR (‘initial TWR’). This is fortunate, since such a movement is experienced very commonly, for example, when one nods the head while walking around a corner. Next we explore whether initial TWR responses are indeed reduced compared to steady-state responses (hypothesis #2).

In theory, initial TWR differs from steady-state TWR in two respects. First, the yaw component of the rotation signal provided by the canals is veridical, since it has not decreased yet (Fig. 2d). Second, as shown in Fig. 2e, the ‘induced’ rotation signal is weaker (62%, see Supplementary Modeling) during initial TWR than during steady-state. If the erroneous acceleration during TWR was a consequence of the induced rotation signal alone, then the initial TWR should induce a substantial linear acceleration (62% as strong as during steady-state). In contrast, the theoretical framework shown in Fig. 3a predicts that initial TWR should not induce any translation signal (because the direction of Ω(t) is veridical; Supplementary Movie 1a).

Like steady-state, the initial induced aVOR (Fig. 7a) also followed precisely the dependence predicted by model simulations, although the latter was half as large as the former (Fig. 7a; see also Fig. 2e). A large difference between initial and steady-state responses was also seen for the induced tVOR: Although small and short-lasting during the first tilt movement, horizontal eye velocity (tVOR) was strong during steady-state (Fig. 7b; see also Fig. 6b).

Fig. 7c compares the PD neuronal population responses to initial and steady-state TWR. Like the tVOR (Fig. 7b), but unlike the induced aVOR (Fig. 7a), the initial TWR elicited only a small response, which was not significantly different from baseline firing for most time samples, in line with model simulations (Fig. 7c). We measured the increase in firing rate within a 1s interval following the actual tilt movement on a cell-by-cell basis. If this response was driven by the induced rotation signal alone (without an internal model), we would expect the cells’ firing rates to be 62% as large during initial TWR as during steady-state TWR. In contrast, we found that the neuronal responses to initial TWR were, at the population level, only 25% as large as the responses to steady-state TWR (linear regression, slope = 0.25 ± 0.05, SE; Fig 8a). The slopes were identical for nodulus/uvula (n = 27, slope:

0.24±0.14, 95% CI) and cerebellar nuclei (n = 31, slope: 0.16±0.15) neurons (see also Supplementary Fig. 5).

That the initial TWR responses are suppressed provides further support for the hypothesis that these cerebellar responses result from processing through an internal model that uses three-dimensional signals from all semicircular canals, as necessary to implement equation (3). This finding has been further quantified by measuring how TWR responses increase as a function of time from EVAR onset (Fig. 8b). The experimental data fell close to a simulation based on the internal model (solid red line) and didn't match a simulation that assumes that the response is proportional to the induced aVOR (and no internal model, broken red line). Altogether, these data show that cerebellar translation-selective neurons encode a neural estimate of the erroneous linear acceleration, whose magnitude follows the decrease of the yaw rotation signal, as predicted by theory.

Discussion

We have used TWR stimuli to show that translation-selective cerebellar cells also encode an erroneous linear acceleration, even when no actual translation occurs. Neural response properties followed theoretical predictions whereby the brain generates an internal estimate of translation as the difference between the net otolith signal and the output of an internal model of gravity[11–19]. In fact, simulations of a simple model that captures these ideas result in predicted erroneous linear acceleration signals that are quantitatively similar to responses of translation-selective cerebellar neurons.

Using a similar experimental protocol, a previous study[5] has shown that erroneous translation estimates can be measured in human tVOR responses. The illusion of induced tilt during TWR has also been measured in humans[5,36]. In contrast, direct evaluation of translation perception during TWR-like stimuli is difficult given the disorienting, confusing and nauseogenic nature of these movements in humans (but see[64]). It is unclear whether the confusion and disorientation experienced by humans during TWR masks the perception of linear acceleration or whether the translation signals are the cause of confusion and disorientation. It is for this reason that we, like others[5], have focused on eye movements rather than perception as a behavioral correlate of the postulated linear acceleration signal.

The conclusion that responses of these cerebellar neurons during TWR reflect their sensitivity to a centrally-generated translation signal has been based on the following observations: First, steady-state TWR responses were significantly correlated with the cell's gain during actual translation (Fig. 5b,c) and, there were no tilt-evoked responses in the absence of EVAR, a stimulus that does not elicit an erroneous translation signal (Fig. 5d). Second, steady-state TWR responses matched the translation signal predicted by the internal model hypothesis in both magnitude (Fig. 5b and 6a) and dynamics (Fig. 6a). Third, variations among animals were satisfactorily predicted by differences in the dynamics of the central processing of rotation signals, which are well understood[5,17,44] and quantified from reflexive eye movements (induced aVOR; Fig. 6c). Finally, the magnitude of this tilt-evoked TWR activity was negligible in the early part of each trial (initial TWR), but gradually increased with time, with a time constant of ~14s (Fig. 8).

This latter finding is particularly intriguing when compared to model predictions. According to the internal model hypothesis, conceptualized by equation (3), the brain has access to an accurate estimate of three-dimensional angular velocity, Ω(t). The suppressed neural response to initial TWR suggests that the brain indeed uses signals from both the horizontal and vertical semicircular canals to compute a reliable three-dimensional estimate of Ω(t) and, as a consequence, G(t). Thus, even though nodulus/uvula Purkinje cells do not modulate during yaw rotations[22,27,45,46], their responses carry an explicit and functionally important yaw rotation signal. The present findings provide an explanation for the puzzling finding that, although nodulus/uvula Purkinje cells do not modulate during yaw rotation, there is a substantial mossy fiber input to the nodulus/uvula from the horizontal semicircular canals[45,47–49].

Alternatively, some authors[50] have proposed that the brain computes linear accelerations by filtering otolith signals without contributions from the semicircular canals ("filtering hypothesis"). This proposal can't account for many behavioral and neurophysiological results[5,20–22,41]. The present findings also strongly contradict the filtering hypothesis. Indeed, all stimuli used here activate the otolith organs in exactly the same manner. Therefore, the filtering hypothesis would predict that TWR shouldn't generate any erroneous translation estimate, which is contrary to our findings (both neural responses and eye movements).

Because of the dynamics of the semicircular canals, however, an accurate angular velocity signal cannot be maintained during constant velocity rotations (Fig. 2d). Thus, during steady-state TWR, the internal estimate of gravity computed by equation (3) would not represent the true angular orientation of the head relative to the world. The output of the internal model would also be different from the net GIA signal carried by otolith afferents (Fig. 1c). Like a pendulum, their difference would then be inferred as a linear acceleration signal (Fig. 1d). The present findings show that activity in nodulus/uvula Purkinje cells and translation-selective cerebellar nuclei neurons precisely reflect the temporal evolution of these signals. The tilt-evoked erroneous translation-like response in these neurons increases with a time constant that is similar to the time constant of decay of angular velocity during the aVOR (Fig. 8b). If the internal model implemented equation (1), inaccuracies and noise in canal-driven angular velocity signals would be detrimental even for natural head movements in everyday life[17]. Like an expert engineer, the brilliant solution our brain has chosen is to add a 'leak' to the vector integration of equation (1), whereby over long intervals the output of the internal model tends to align the internal gravity estimate with the otolith-driven GIA signal (equation 3). In a Bayesian framework, this leak (somatogravic feedback; Fig. 3a) reflects the experience that we are more likely stationary than accelerating in the world[16,17]. Remarkably, the tilt-evoked erroneous translation-like responses are short-lasting (time constant of ~2–3s; Fig. 6a), reflecting the influence of somatogravic feedback.

There is a large literature suggesting that one of the functions of the cerebellum is the implementation of internal models[2,28–31]. While this theory has typically been used to study motor control[6,29–31,46], the 'internal model' concept has been extended to include neural systems that mimic physical principles, as pertinent to sensory processing[2,5]. The present

findings support further the notion that the cerebellum and its targets are involved in the implementation of these theoretical concepts. However, they cannot determine whether the underlying computations are actually occurring within the cerebellum. Preliminary experiments, however, suggest that translation-selective nodulus/uvula Purkinje cells lose their ability to distinguish tilt from translation following local gabazine injections (Yakusheva, T.A., Angelaki, D.E., and Blazquez P.M., unpublished observations), suggesting that it is possible that these internal model computations utilize gabaergic circuitry within the cerebellar cortex.

Materials and Methods

Animals and Experimental Setup

Three male rhesus monkeys V, T and K (Maccaca mulatta, 6, 4 and 8 years old respectively), which were chronically implanted with a single scleral search coil to measure horizontal and vertical eye movements[51,52], were used for neural recordings. Two additional animals (P and N, both 5 years old) implanted with a dual eye coil were used for three-dimensional (horizontal, vertical and torsional) eye movement recordings only. All animals were also implanted with a circular delrin ring to immobilize the head and a delrin platform with staggered rows of holes for neural recordings. To provide better access to the midline of the cerebellum, the platform was tilted leftward 10° in two of the animals (T and K); in the third animal (V), the platform had a double-angle: it was tilted both rightward 10° and forward 10°. Animals P and N were. All experimental procedures were in accordance with US National Institutes of Health guidelines and approved by the Animal Studies Committee. Animals were pair-housed under natural dark-light cycle. Animal T and K had no prior history of testing; animals P and N were used for cortical recording studies; animal V was used for other neurophysiology studies, including injections of a reversible GABA antagonist (gabazine).

During experiments animals were comfortably seated in a primate chair secured inside the inner gimbal of a vestibular stimulator composed of a three-axis rotator mounted on a 2 m linear sled (Acutronics Inc., Pittsburgh, PA). The first two axes allowed tilting the animal in any orientation, and the third axis rotated the setup around an earth-vertical axis. The animals were positioned such that all three rotation axes were aligned with the center of the head and the stereotaxic-horizontal plane was earth-horizontal. The eye coil signals and the stimuli were filtered (200Hz; 6-pole Bessel) and digitized at a rate of 833.33 Hz (model 1401, CED, 16-bit resolution; Cambridge Electronics Design, Cambridge, UK).

Neural Recordings

Cerebellar nuclei neurons and Purkinje cells in the nodulus (lobule 10) and uvula (lobule 9) (collectively referred to here as ‘nodulus/uvula’) were recorded extracellularly using epoxy coated tungsten microelectrodes (9–12 MΩ impedance; FHC, Bowdoinham, ME) through 26-gauge guide tubes. Neuronal data was acquired using an analog channel of the 1401 (33 KHz) and analyzed offline using a custom Matlab (Mathworks) script to extract spike timing from the raw neuronal data. We sorted spikes manually based on spike statistics (amplitude, peak velocity) and principal component analysis.

The cerebellar nuclei and nodulus/uvula were identified using stereotaxic coordinates, as well as the location of the abducens nuclei in each animal (Supplementary Fig. 2). All nodulus/uvula data included in this analysis were recorded from the Purkinje cell layer, where both simple spikes and complex spikes could be recorded simultaneously. We tested offline whether SS activity paused for at least 10ms following each complex spike: nodulus/uvula cells where this pause was observed were classified as 'confirmed' Purkinje cells; otherwise they were classified as 'putative' Purkinje cells. Cerebellar nuclei recordings were performed in regions directly dorsal to the nodulus/uvula. Therefore, they were presumably located mainly in the fastigial nuclei, although recordings could have extended into the interposed nuclei. These anatomical landmarks have been extensively used and verified in previous experiments [22,26,27]. All recordings were performed with all room lights turned off and in complete darkness.

Experimental Protocols

Upon isolation of each cell, we first measured its responses to combinations of 0.5 Hz tilt and translation, which were identical to the stimuli used in[9,20–22,27]. These stimuli consisted of either pure tilt ('tilt'), pure translation ('translation') or combined translation and tilt ('tilt −translation' and 'tilt + translation'). The tilt stimulus was a 0.5 Hz sinusoidal rotation around upright with peak amplitude of 11.5° (and peak velocity of 36°/s). Because this motion reorients the head relative to gravity, otolith afferents were stimulated by a 0.5 Hz gravitational acceleration component in the horizontal plane with a peak magnitude of 2 m/s^2 (0.2G). The amplitude of the translation stimulus (20 cm) was adjusted so that the inertial acceleration of 0.2 G matched the horizontal gravitational acceleration during the tilt stimulus. During combined rotation and translation stimuli, inertial and gravitational acceleration components combined in either an additive or subtractive fashion depending on the relative directions of the two stimuli. As a result, the net GIA activating the otolith receptors either doubled (tilt + translation) or was nearly zero (tilt − translation), even though the actual translation of the animal remained the same[9].

These stimuli were used to first identify translation-selective cells and then evaluate which of 4 directions (naso-occipital (NO), interaural (IA) and 45° in-between axes) gave the largest response. TWR movements were then delivered along the direction with the largest translation response. Although cells were tested along any one of these 4 directions, for simplicity the model and stimuli (Fig. 1–3) are described such as if TWR were always delivered along the NO axis (i.e., using pitch tilts). Axes and sign conventions were as follows: Positive directions for the three head axes are forward (NO), leftward (IA) and upward (vertical axis). Yaw, pitch and roll rotations are defined around the vertical, IA and NO axis (positive directions: leftward, nose-down and right-ear-down, respectively).

Each TWR run was composed of a series of 10° tilt movements performed during a single period of constant-velocity earth-vertical axis rotation (EVAR), as follows (Fig. 1): The animal was first statically tilted 10° in either one direction perpendicular to the axis with the largest translation response. Ten seconds later and while the animal remained in the tilted orientation, constant velocity EVAR (velocity: 45°/s and/or 120°/s; acceleration: $45°/s^2$) was subsequently delivered. As soon as the constant velocity was reached (1s after EVAR onset

for 45°/s and 2.6s for 120°/s), the first tilt movement (towards the opposite 10° position) was initiated (Fig. 2a–c). A total of 8 tilt movements were performed, separated by intervals of 30s. Each movement reversed the direction of tilt and followed a trapezoidal velocity profile (peak acceleration 50°/s^2, peak velocity 20°/s, total duration 1.4s; Fig. 2b,c; see also Supplementary Fig. 3–6). Thirty seconds after the last tilt movement, the EVAR was stopped. After a resting period of at least 30s, the animal was brought back smoothly to a new initial position and another run was initiated. At least 4 TWR runs were performed with opposite initial tilt directions (as in Supplementary Fig. 3) and leftward/rightward EVAR (as in Fig. 4). In addition, one control run was performed during which tilt movements were applied without any EVAR (Fig. 4e). In the following, we refer to each discrete tilt movement as a 'trial'.

Sample size

For these experiments, we specifically searched for translation-responsive cells. This was done by qualitatively comparing tilt and translation responses on-line. We then used the same principles as in[9] to identify translation-selective cells quantitatively offline (see Data analyses). In total we recorded from 40 cerebellar nuclei and 38 nodulus/uvula cells, of which 31 cerebellar nuclei and 30 nodulus/uvula cells (16 were 'confirmed' and 14 were 'putative' Purkinje cells) were classified as translation-selective neurons offline. Only the latter group of cells has been included in the present analyses. Responses to 45°/s responses were available for 58 cells (31 cerebellar nuclei, 27 nodulus/uvula).

Responses to TWR at 120°/s were available in 11 cells (6 cerebellar nuclei, 5 PC) from animal T only (Animals V and K were heavier (9.2 kg and 10 kg respectively) than animal T (5.3 kg), and therefore our setup could not perform TWR at 120°/s in these animals). We compared (Supplementary Fig. 5) the responses of cerebellar nuclei, 'confirmed' and 'putative' PC and found no difference. Therefore, we pooled all data together for the main analyses. To investigate how responses depend on the time between the beginning of EVAR and the tilt movement, additional TWR runs (at 45°/s) were also delivered in a subset of cells (n=11) for which the first tilt movement occurred 5, 10, 15 or 20s after the beginning of EVAR.

Data analyses

Neural Responses—Responses to tilt and translation were analyzed offline using a variant of the partial correlation analysis previously employed to test whether neurons selectively encode translation, tilt or GIA[9,22]. Cells were classified as 'translation-selective' if the translation model fitted their activity significantly better ($p < 0.05$), and were excluded from the present study otherwise. For cells that passed this test, the response to 0.5 Hz translation (in units of spikes.s^{-1} per m.s^{-2}) was used as a reference to characterize TWR responses quantitatively (see below).

To quantify TWR responses, we first separated 'trials' based on whether model predictions should generate a linear acceleration in the cell's preferred direction (PD) or anti-PD. Based on the sign conventions adopted here, model predictions for the direction of the induced linear acceleration depended on both the direction of tilt and the direction of EVAR. For

example, a positive tilt movement around any axis (e.g., pitch, see Fig. 2) during positive (e.g., leftward) EVAR was predicted to induce a positive acceleration along that axis (e.g., leftward). Similarly, a negative tilt movement during negative EVAR should induce an identical (positive) acceleration signal. We examined whether, during sinusoidal translation, the cell increased its firing rate during acceleration in this direction (i.e. if the peak response occurred while the acceleration was positive). If so, these trials were considered to be in the cell's PD; if not, then they were considered to be in the cell's anti-PD. Similarly, we determined if the responses measured following negative tilt during positive EVAR and positive tilt during negative EVAR were in PD or anti-PD.

Eye movements—Simultaneously with the analyses of neural responses, we also quantified calibrated and de-saccaded eye position signals. Slow phase eye velocity was computed using digital differentiation, filtering and de-saccading[15,53]. The magnitude and dynamics of the tVOR depends strongly on the direction of linear acceleration and vergence angle[54]. Specifically, lateral linear accelerations evoke a horizontal tVOR in darkness, whereas conjugate horizontal slow phase eye velocity is negligible for fore-aft movements[54]. Thus, only pitch TWR runs (Supplementary Fig. 3b), but not roll TWR runs (Supplementary Fig. 3e), produce an observable conjugate tVOR in darkness. Because of this property, it is possible to separate the tVOR from the yaw aVOR, using a similar method as in[5] (see Supplementary Fig. 3 for details).

Statistical analysis—Data during steady-state TWR (i.e. when tilt was delivered more than 30 s after the beginning of TWR) were analyzed first. For each cell, we averaged responses during all trials in PD and anti-PD. We measured the difference between the average firing rate over 1 s intervals immediately before the onset and after the offset of each tilt movement (Fig. 5a). This firing rate change was then plotted as a function of the cell's sensitivity to sinusoidal translation and the Matlab function regress was used to search for correlation between the two response parameters. We confirmed that our sample is adequate for performing parametric statistics (i.e. linear regression and Student statistics) by replicating all analyses after applying a method which identifies and removes outliers (Matlab function robustfit) and finding that the results were unaffected.

Correlations between the cell's sensitivity to sinusoidal translation and its response to TWR were evaluated by performing linear regression and F-tests. We computed the average firing rate following TWR in PD, anti-PD and control; 95% confidence intervals were computed using Student statistics (i.e. as the standard deviation of the firing rate across cells multiplied by $t_{0.05,n-1}/\mathrm{sqrt}(n-1)$, where $t_{0.05,n-1}$ is the critical value of the Student distribution with n–1 degrees of freedom and n is the number of cells). All tests performed in the study were two-sided. All tests that yielded statistically significant results had very small p-values ($<10^{-4}$), which compensated the effect of performing multiple comparisons.

The time course of the tilt-induced responses in translation-selective cells were also computed from TWR runs with tilt movements occurring 1–60 s after the onset of EVAR (see Experimental Protocols). This was done by computing correlation slopes with steady-state responses. These slope values were plotted as a function of time, and the time constant was quantified by an exponential fit using a gradient ascent procedure (function lsqnonlin,

Matlab). The confidence interval of the exponential fit was computed by bootstrapping[55]. Note that the 95% CIs computed for the time constant are large because exponential fits on a small number of samples can be quite variable.

Modeling—For comparisons with experimental data, we have also simulated a previously published model[17], whose schematic is illustrated in Fig. 3a. This model can be seen as a synthesis of multiple studies based on the internal model hypothesis[11–19]. This model is also inspired by and consistent with another published model based on the Bayesian approach[16].

Finally, simultaneously recorded eye movements were used to set the model parameters, under the assumption that they reflect signals proportional to the internal variables of induced tilt and translation signals (as previously shown[5]). Note that, when the 5 model parameters were set such that they reproduced the behavioral responses satisfactorily (e.g., Fig. 6c and 7a), the model also simulated the neuronal responses accurately. Note also that the tVOR slow phase eye velocity likely reflects further filtering beyond an internal estimate of linear acceleration[42,56] (Supplementary Fig. 6), which were not included in the 5-parameter model of Fig. 3. Details about the model and the parameters used for simulations can be found in Supplementary Modeling.

Supplementary Material

Refer to Web version on PubMed Central for supplementary material.

Acknowledgments

This work was supported by NIH grant EY12814. We would like to thank Eliana Klier, Pablo Blazquez and Tanya Yakusheva for critically reading this manuscript.

References

1. Berkes P, Orbán G, Lengyel M, Fiser J. Spontaneous cortical activity reveals hallmarks of an optimal internal model of the environment. Science. 2011; 331:83–87. [PubMed: 21212356]
2. Cullen KE, Brooks JX, Jamali X, Carriot J, Massot C. Internal models of self-motion: computations that suppress vestibular reafference in early vestibular processing. Exp Brain Res. 2011; 210:377–388. [PubMed: 21286693]
3. Indovina I, Maffei V, Bosco G, Zago M, Macaluso E, Lacquaniti F. Representation of visual gravitational motion in the human vestibular cortex. Science. 2005; 308(5720):416–9. [PubMed: 15831760]
4. Keller GB, Hahnloser RH. Neural processing of auditory feedback during vocal practice in a songbird. Nature. 2009; 457:187–90. [PubMed: 19005471]
5. Merfeld DM, Zupan LH, Peterka RJ. Humans use internal models to estimate gravity and linear acceleration. Nature. 1999; 398:615–618. [PubMed: 10217143]
6. Shadmehr R, Mussa-Ivaldi FA. Adaptive representation of dynamics during learning of a motor task. J Neurosci. 1994; 14:3208–3224. [PubMed: 8182467]
7. Zago M, McIntyre J, Senot P, Lacquaniti F. Internal models and prediction of visual gravitational motion. Vision Res. 2008; 48(14):1532–8. [PubMed: 18499213]
8. Einstein A. Über das Relativitätsprinzip und die aus demselben gezogenen Folgerungen. Jahrbuch der Radioaktivität und Elektronik. 1907; 4:411–462.
9. Angelaki DE, Shaikh AG, Green AM, Dickman JD. Neurons compute internal models of the physical laws of motion. Nature. 2004; 430:560–564. [PubMed: 15282606]

10. Fernández C, Goldberg JM, Abend WK. Response to static tilts of peripheral neurons innervating otolith organs of the squirrel monkey. J Neurophysiol. 1972; 35:978–987. [PubMed: 4631840]
11. Bos JE, Bles W. Theoretical considerations on canal-otolith interaction and an observer model. Biol Cybern. 2002; 86:191–207. [PubMed: 12068786]
12. Green AM, Angelaki DE. An integrative neural network for detecting inertial motion and head orientation. J Neurophysiol. 2004; 92:905–925. [PubMed: 15056677]
13. Green AM, Shaikh AG, Angelaki DE. Sensory vestibular contributions to constructing internal models of self-motion. J Neural Eng. 2005; 2:S164–179. [PubMed: 16135882]
14. Holly JE. Vestibular coriolis effect differences modeled with three-dimensional linear-angular interactions. J Vestib Res. 2004; 14:443–460. [PubMed: 15735327]
15. Laurens J, Strauman D, Hess BJ. Spinning versus wobbling: how the brain solves a geometry problem. J Neurosci. 2011; 31:8093–101. [PubMed: 21632931]
16. Laurens J, Droulez J. Bayesian processing of vestibular information. Biol Cybern. 2007; 96:389–404. [PubMed: 17146661]
17. Laurens J, Angelaki DE. The functional significance of velocity storage and its dependence on gravity. Exp Brain Res. 2011; 210:407–422. [PubMed: 21293850]
18. Merfeld DM. Modeling the vestibulo-ocular reflex of the squirrel monkey during eccentric rotation and roll tilt. Exp Brain Res. 1995; 106:123–134. [PubMed: 8542968]
19. Zupan LH, Merfeld DM, Darlot C. Using sensory weighting to model the influence of canal, otolith and visual cues on spatial orientation and eye movements. Biol Cybern. 2002; 86:209–230. [PubMed: 12068787]
20. Angelaki DE, McHenry MQ, Dickman JD, Newlands SD, Hess BJ. Computation of inertial motion: neural strategies to resolve ambiguous otolith information. J Neurosci. 1999; 19:316–327. [PubMed: 9870961]
21. Shaikh AG, Green AM, Ghasia FF, Newlands SD, Dickman JD, Angelaki DE. Sensory convergence solves a motion ambiguity problem. Curr Biol. 2005; 15:1657–1662. [PubMed: 16169488]
22. Yakusheva T, Shaikh AG, Green AM, Blazquez PM, Dickman JD, Angelaki DE. Purkinje cells in posterior cerebellar vermis encode motion in an inertial reference frame. Neuron. 2007; 54:973–985. [PubMed: 17582336]
23. Liu S, Angelaki DE. Vestibular signals in macaque extrastriate visual cortex are functionally appropriate for heading perception. J Neurosci. 2009; 29:8936–8945. [PubMed: 19605631]
24. Liu S, Dickman JD, Angelaki DE. Response dynamics and tilt versus translation discrimination in parietoinsular vestibular cortex. Cereb Cortex. 2011; 21:563–573. [PubMed: 20624839]
25. Meng H, May PJ, Dickman JD, Angelaki DE. Vestibular signals in primate thalamus: properties and origins. J Neurosci. 2007; 27:13590–13602. [PubMed: 18077671]
26. Angelaki DE, Yakusheva TA. How vestibular neurons solve the tilt/translation ambiguity. Comparison of brainstem, cerebellum, and thalamus. Ann N Y Acad Sci. 2009; 1164:19–28. [PubMed: 19645876]
27. Yakusheva T, Blazquez PM, Angelaki DE. Frequency-selective coding of translation and tilt in macaque cerebellar nodulus and uvula. J Neurosci. 2008; 28:9997–10009. [PubMed: 18829957]
28. Lisberger SG. Internal models of eye movement in the floccular complex of the monkey cerebellum. Neuroscience. 2009; 162(3):763–76. [PubMed: 19336251]
29. Pasalar S, Roitman AV, Durfee WK, Ebner TJ. Force field effects on cerebellar Purkinje cell discharge with implications for internal models. Nat Neurosci. 2006; 9:1404–11. [PubMed: 17028585]
30. Wolpert DM, Ghahramani Z, Jordan MI. An internal model for sensorimotor integration. Science. 1995; 269:1880–1882. [PubMed: 7569931]
31. Shadmehr R, Krakauer JW. A computational neuroanatomy for motor control. Exp Brain Res. 2008; 185:359–381. [PubMed: 18251019]
32. Bles W. Coriolis effects and motion sickness modeling. Brain Res Bull. 1998; 47:543–549. [PubMed: 10052586]

33. DiZio P, Lackner JR, Evanoff JN. The influence of gravitoinertial force level on oculomotor and perceptual responses to Coriolis, cross-coupling stimulation. Aviat Space Environ Med. 1987; 58:A218–223. [PubMed: 3675495]
34. Guedry FE, Montague EK. Quantitative Evaluation of the Vestibular Coriolis Reaction. Aerospace Med. 1961; 32:487–500.
35. Kennedy RS, Tolhurst GC, Graybiel A. The effects of visual deprivation on adaptation to a rotating environment. NSAM-918 Res Rep US Naval School of Aviation Medicine. 1965; 18:1–36.
36. Tribukait A, Eiken O. Changes in the perceived head transversal plane and the subjective visual horizontal induced by Coriolis stimulation during gondola centrifugation. J Vestib Res. 2006; 16:105–116. [PubMed: 17312338]
37. Hess BJ, Angelaki DE. Angular velocity detection by head movements orthogonal to the plane of rotation. Exp Brain Res. 1993; 95:77–83. [PubMed: 8405254]
38. Goldberg JM, Fernandez C. Physiology of peripheral neurons innervating semicircular canals of the squirrel monkey. I Resting discharge and response to constant angular accelerations. J Neurophysiol. 1971; 34:635–660. [PubMed: 5000362]
39. Raphan, T.; Cohen, B.; Matsuo, V. A velocity storage mechanism responsible for optokinetic nystagmus (OKN), optokinetic after-nystagmus (OKAN) and vestibular nystagmus. In: Baker, R.; Berthoz, A., editors. Control of gaze by brain stem neurons. Elsevier; Amsterdam: 1977. p. 37-47.
40. Shaikh AG, Meng H, Angelaki DE. Multiple reference frames for motion in the primate cerebellum. J Neurosci. 2004; 19:4491–7. [PubMed: 15140919]
41. Shaikh AG, Ghasia FF, Dickman JD, Angelaki DE. Properties of cerebellar fastigial neurons during translation, rotation, and eye movements. J Neurophysiol. 2005; 93:853–863. [PubMed: 15371498]
42. Miles FA, Fuller JH, Braitman DJ, Dow BM. Long-term adaptive changes in primate vestibuloocular reflex. III Electrophysiological observations in flocculus of normal monkeys. J Neurophysiol. 1980; 43:1437–1476. [PubMed: 6768853]
43. Green AM, Galiana HL. Hypothesis for shared central processing of canal and otolith signals. J Neurophysiol. 1998; 80:2222–2228. [PubMed: 9772275]
44. Laurens J, Straumann D, Hess BJ. Processing of angular motion and gravity information through an internal model. J Neurophysiol. 2010; 104:1370–1381. [PubMed: 20610780]
45. Barmack NH, Shojaku H. Vestibular and visual climbing fiber signals evoked in the uvula-nodulus of the rabbit cerebellum by natural stimulation. J Neurophysiol. 1995; 74:2573–2589. [PubMed: 8747215]
46. Bo J, Block HJ, Clark JE, Bastian AJ. A cerebellar deficit in sensorimotor prediction explains movement timing variability. J Neurophysiol. 2008; 100(5):2825–32. [PubMed: 18815350]
47. Newlands SD, Vrabec JT, Purcell IM, Stewart CM, Zimmerman BE, Perachio AA. Central projections of the saccular and utricular nerves in macaques. J Comp Neurol. 2003; 466:31–47. [PubMed: 14515239]
48. Korte GE, Mugnaini E. The cerebellar projection of the vestibular nerve in the cat. J Comp Neurol. 1979; 184:265–277. [PubMed: 762284]
49. Maklad A, Fritzsch B. Partial segregation of posterior crista and saccular fibers to the nodulus and uvula of the cerebellum in mice, and its development. Brain Res Dev Brain Res. 2003; 140:223–236. [PubMed: 12586428]
50. Raphan T, Cohen B. The vestibulo-ocular reflex in three dimensions. Exp Brain Res. 2002; 145:1–27. [PubMed: 12070741]
51. Meng H, Green AM, Dickman JD, Angelaki DE. Pursuit-vestibular interactions in brain stem neurons during rotation and translation. J Neurophysiol. 2005; 93:3418–3433. [PubMed: 15647394]
52. Meng H, Angelaki DE. Neural correlates of the dependence of compensatory eye movements during translation on target distance and eccentricity. J Neurophysiol. 2006; 95:2530–40. [PubMed: 16407428]
53. Holden JR, Wearne SL, Curthoys IS. A fast, portable desaccading program. J Vestib Res. 1992; 2:175–179. [PubMed: 1342392]

54. Angelaki DE, Hess BJM. Self-motion induced eye movements: Effects on visual acuity and navigation. Nat Rev Neurosci. 2005; 6:966–976. [PubMed: 16340956]

55. Efron B, Tibshirani R. Statistical data analysis in the computer age. Science. 1991; 253:390–395. [PubMed: 17746394]

56. Green AM, Angelaki DE. Resolution of sensory ambiguities for gaze stabilization requires a second neural integrator. J Neurosci. 2003; 23(28):9265–75. [PubMed: 14561853]

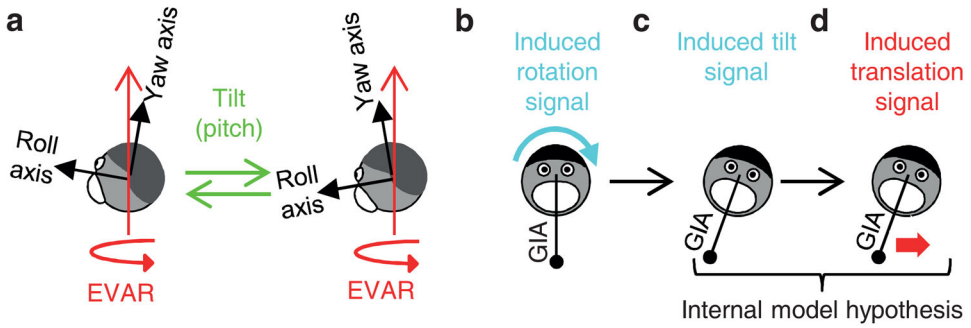

Figure 1. Schematic illustrating the Tilt-While-Rotating (TWR) stimulus

(a) Constant velocity earth-vertical axis rotation (EVAR, red arrow), superimposed on nose-up and nose-down pitch tilt. The yaw and roll axes of the head are represented by black arrows. **(b)–(d)** Representation of the induced roll rotation, the resulting head tilt estimate and the erroneous translation signal induced during steady-state TWR. The gravito-inertial acceleration (GIA) sensed by the otolith organs is represented by a pendulum. Only in the presence of a linear acceleration (translation signal, red arrow), such as shown in Fig. 1d, a pendulum would remain aligned with the head/body vertical axis while tilted.

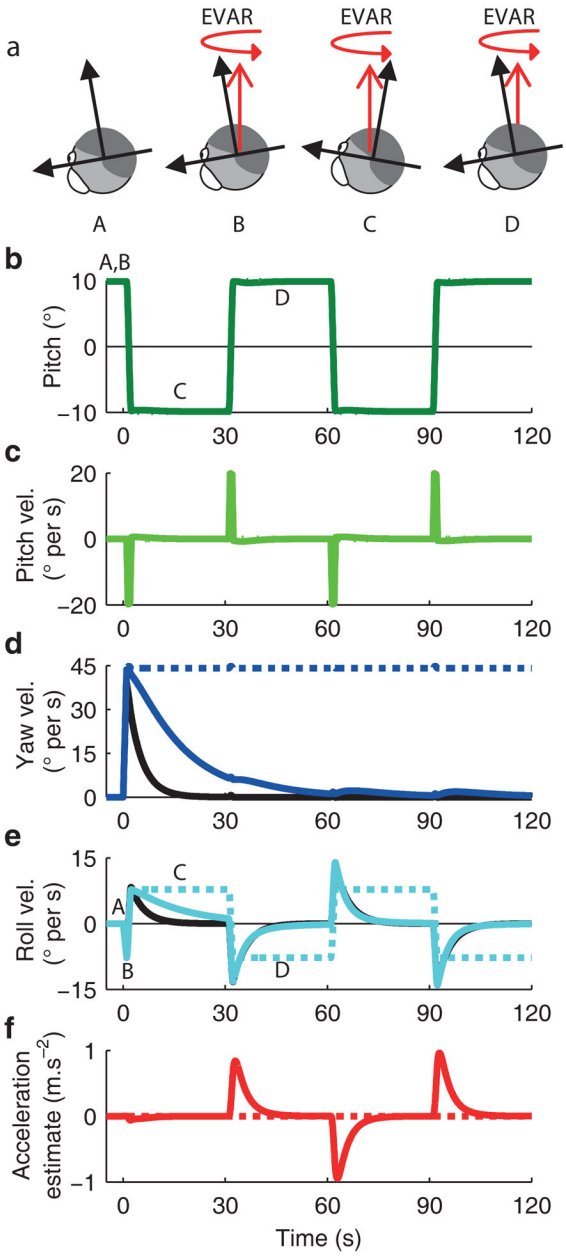

Figure 2. Motion signals during TWR

(a) Illustration of the sequence of motion during the TWR stimulus: The head is initially tilted (A). The EVAR (red arrow) starts at t = 0 (B), and a tilt movement is performed immediately thereafter (t = 1s) (C). A second tilt movement is performed 30 s later (D). **(b), (c)** Sequence of pitch tilt position and velocity (green). **(d), (e)** Yaw and roll (induced) angular velocity (see also Supplementary Fig. 4). Black lines represent the rotation signal coded by the canals. Blue (**d**) or cyan (**e**) solid lines represent the simulated central rotation signal (velocity storage). Because the canals are sensitive to changes in velocity, each ±10° pitch tilt (green) induces a 15.6°/s roll rotation signal (cyan). Note that this induced roll rotation signal is smaller during the first tilt because of the larger yaw rotation signal (see

Supplementary Modeling for details). **(f)** Simulated linear acceleration (translation) signal (red). Dotted lines: real motion of the head (egocentric reference frame).

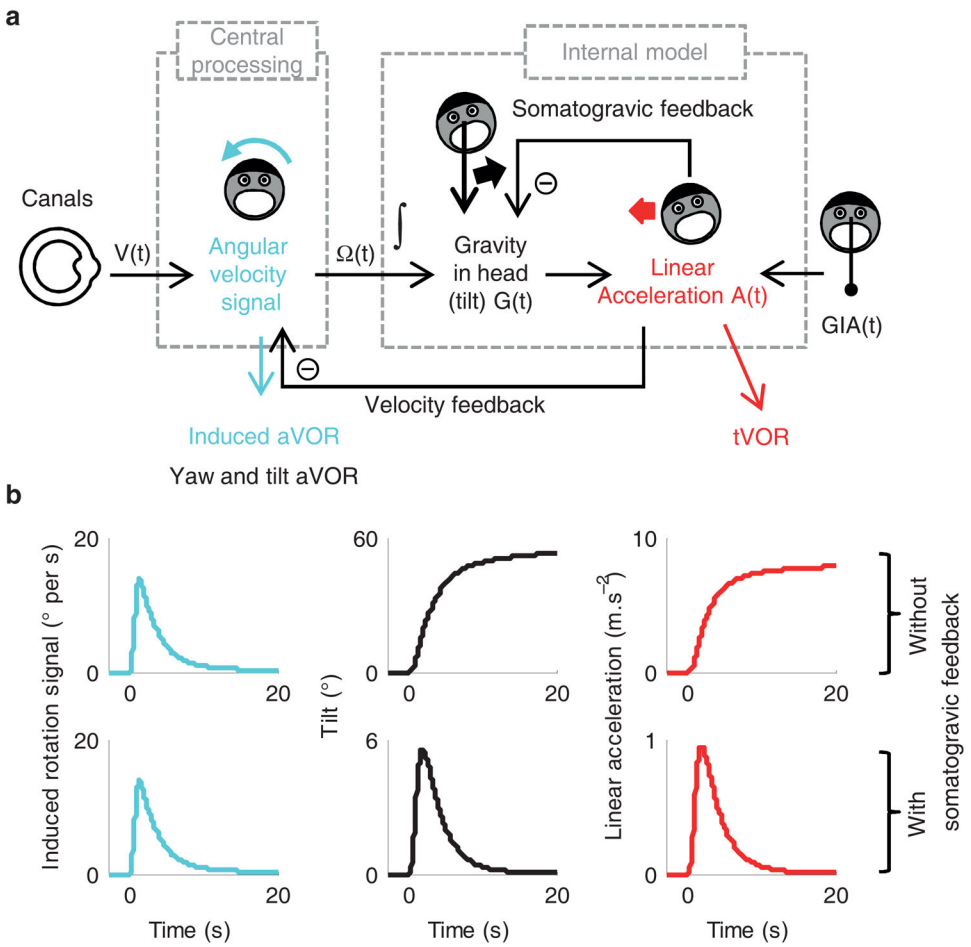

Figure 3. Model schematic and simulations

(a) Model outline and **(b)** simulations of induced tilt velocity (left column, cyan), induced tilt position (middle column, black) and induced linear acceleration (right column, red) during steady-state TWR. Simulations in (**b**) are shown without (upper row, equation 1) or with (lower row, equation 3) the somatogravic feedback. Details about the model (with 5 parameters), which represents a synthesis of several previous studies[11–19], can be found in[17] (see also Supplementary Modeling).

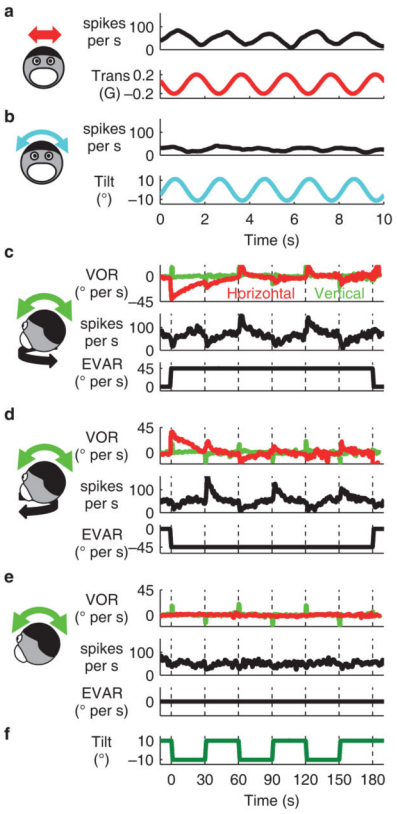

Figure 4. Response from a translation-selective Purkinje cell during

(a) actual lateral translation (0.5 Hz), **(b)** actual roll tilt (0.5 Hz), **(c),(d)** TWR (pitch tilt during leftward and rightward EVAR at 45°/s, respectively) and **(e)** pitch tilt alone. **(f)** shows tilt position timing. Note the transient horizontal VOR (red) and firing rate changes (FR, black) in (**c**) and (**d**) (but not **e**) after each tilt movement (vertical dashed lines). In (**a**), the cell fires maximally when the acceleration is negative. Because negative pitch movements (i.e. towards nose-up) during positive (leftward) EVAR (**c**) and positive pitch movements during rightward EVAR (**d**) induce a negative acceleration (see Fig. 1 and 2), these movements were defined as being along the cell's preferred direction (PD). Accordingly, they resulted in a firing rate increase during TWR. Note the difference in response as a function of time: The first tilt resulted in a weak firing rate decrease, instead of large firing rate increases (**c**) and decreases (**d**) seen for later movements.

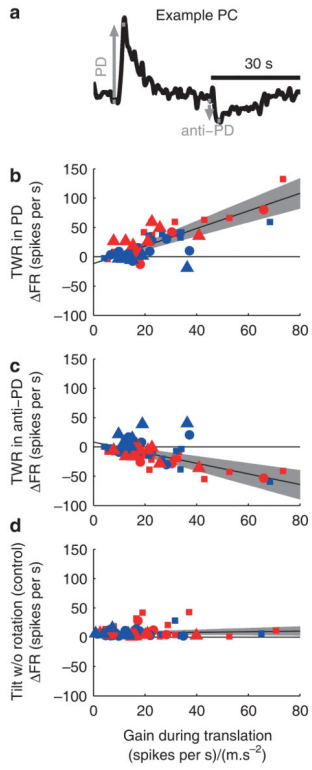

Figure 5. Quantification of firing rate changes during TWR at 45°/s in preferred and anti-preferred directions

(a) Schematic illustrating definition of response along preferred direction (PD, shown in **b**) and anti-PD (shown in **c**). PD is defined as the tilt/EVAR combination that would theoretically elicit an erroneous translation in the preferred direction of the cell (expected to increase firing rate); anti-PD is the opposite direction **(b), (c), (d)** Comparison of firing rate changes (difference between the firing rate averaged over 1 s intervals immediately before the onset and after the offset of each tilt movement) during steady-state TWR in PD (**b**) and anti-PD (**c**), as well as during tilt without EVAR (**c**) vs. the cell's gain during actual translation. In (**d**), PD is not easily defined, thus we plotted the absolute difference between the responses to tilt in both directions. On panels (**b–c**), regression lines are shown in black and confidence intervals are represented by grey bands Blue: cerebellar nuclei cells (n = 31); Red: nodulus/uvula Purkinje cells (n = 27). When separated into cerebellar nuclei and nodulus/uvula, the slopes of the PD response were 1.6 [1.11,1.98, 95% CI] and 0.9 [0.6, 1.4] $m.s^{-2}$, respectively. For the TWR responses in anti-PD, the slopes were −0.7 [−1, − 0.5] and −0.7 [−1.3, −0.15] $m.s^{-2}$, respectively. Different symbols are used for different animals (V: squares, T: circles, K: triangles).

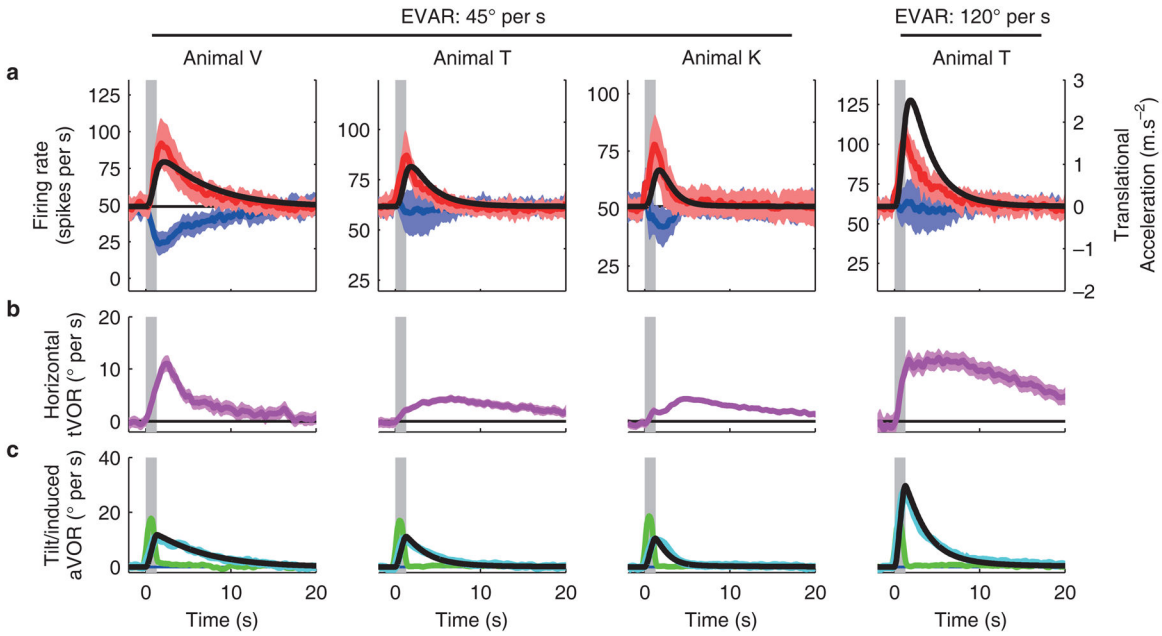

Figure 6. Population responses, eye movements and model simulations during steady-state TWR

(a) Average changes in firing rate (lines) and confidence interval (bands) following tilt in PD (red) or anti-PD (blue) (n = 21, 20 and 17 cells in animals V,T and K at 45°/s, n = 11 in animal T at 120°/s). Superimposed black lines show the simulated estimate of translational acceleration induced by TWR. Neural responses are shown in spikes per s and simulated translation is shown in units of $m.s^{-2}$ (left and right ordinate, respectively). Peak responses in each animal have approximately the same amplitude, ~1.5 $m.s^{-2}$, which matches the slope of the regression line shown in Fig. 5a (as both represent a decoded acceleration signal). **(b)** Horizontal eye velocity that reflects the induced erroneous translation signal[5]. **(c)** Actual tilt aVOR (green) and induced (cyan) vertical aVOR. The confidence intervals are too narrow to be visible. Superimposed black lines show the simulated estimate of the induced tilt signal (scaled by a factor of 0.8 to be compared with the induced aVOR). The tVOR (**b**) and aVOR (**c**) were evaluated using 219, 780 and 1018 trials in animals V,T and K at 45°/s, and 495 in animal T at 120°/s.

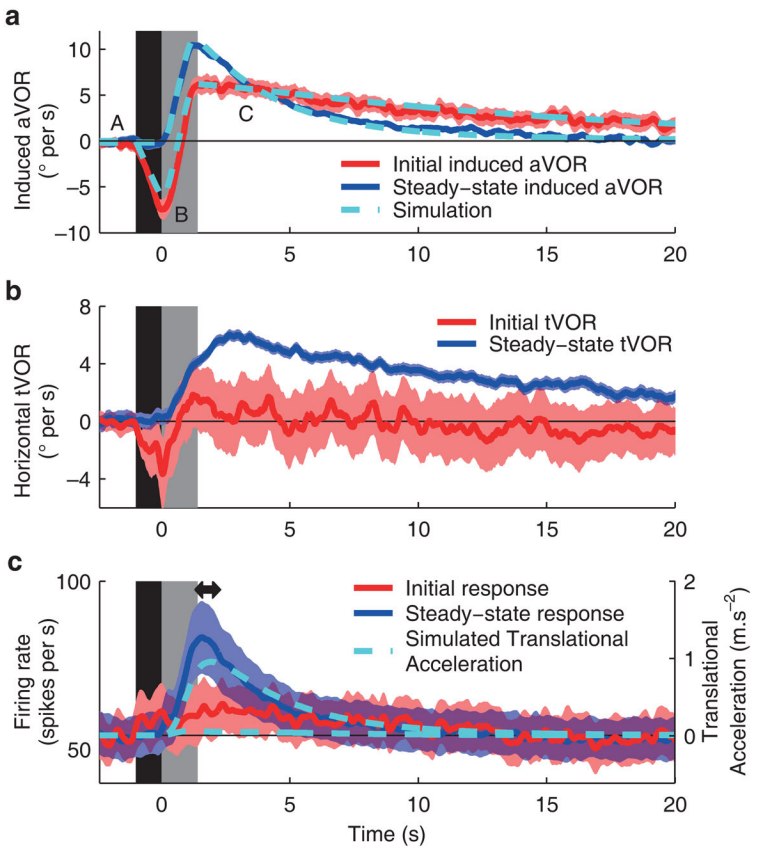

Figure 7. Comparison between initial and steady-state TWR

(a) Induced aVOR, **(b)** induced tVOR and **(c)** average firing rate (n = 58 cells) following initial TWR (red, mean ± confidence interval) and steady-state TWR (blue, mean ± confidence interval), averaged across all animals. For consistency with Fig. 6, the time axis aligned with the beginning of the tilt movement. The period during which the EVAR axis accelerates to 45°/s is indicated by a black band (from t = −1 to t = 0s). The grey band represents the period during which the tilt movement is performed (from t = 0 to t = 1.4s). The simulated induced aVOR velocity signal (from Fig. 2e, cyan), scaled by a factor of 0.8 (in order to account for the gain of the vertical aVOR) is shown for comparison in (**a**) (cyan dashed lines). Similarly, simulations of linear acceleration are superimposed in (**c**) (cyan dashed lines). The sequence of rotation signals (A,B,C) induced at the beginning of TWR (see Fig. 2) is also shown in (**a**). Traces in (**a**) and (**b**) were constructed from 249 (initial TWR) and 2017 (steady-state) trials. The double arrow heads in (**c**) illustrate the 1 s interval used to measure mean firing rate in Fig. 8a.

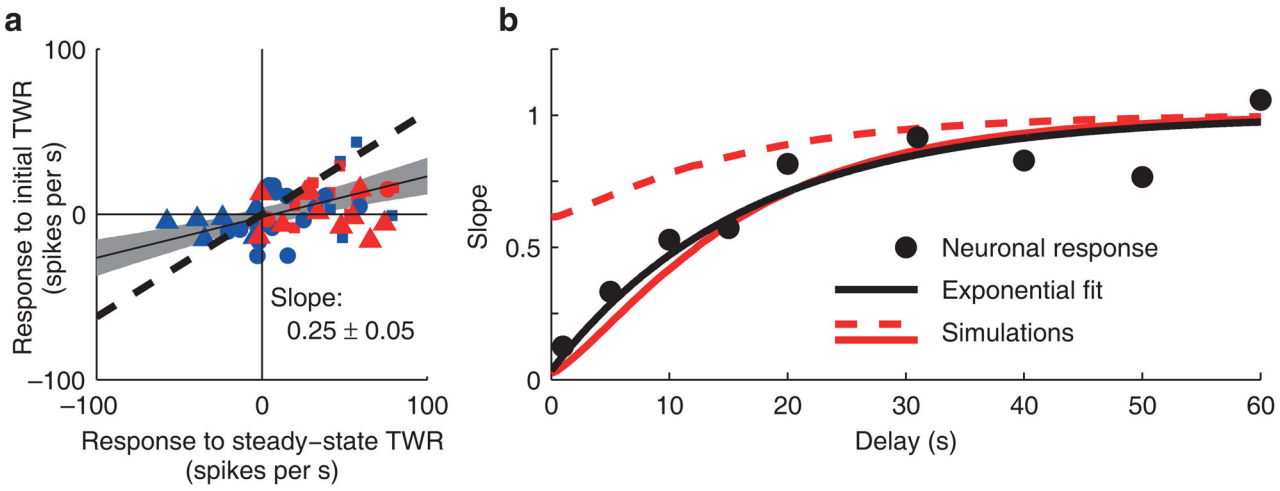

Figure 8. Time dependence of normalized population responses as a function of the delay between the beginning of EVAR and the tilt movement

(a) Comparison of PD neuronal responses to initial TWR and steady-state responses (n = 58 cells; same color code as in Fig. 5). The black line and gray band represent the regression line and its 95% confidence interval. Dashed line: 62% prediction (no internal model). **(b)** Influence of the delay between the tilt movement and the constant velocity rotation onset on the amplitude of the response (n = 11 neurons). Data points show population slope (calculated from regressions as in a). The solid black line shows exponential fit: intercept = −0.01, CI = [−0.35, 0.3], time constant = 14s (similar to the time constant of decay of the horizontal aVOR: 12, 17 and 18 s in animals V, T and K, respectively). The solid red line shows internal model simulation (Fig. 3a). The dashed red line shows the prediction assuming that the response is proportional to the induced aVOR (and no internal model).